

## Phase separation between conductive and insulative materials induced by the electric field

Yuko Nagamine\*

*Department of Intelligent System Engineering, National Institute of Technology, Ube College, Yamaguchi, 755-8555, Japan*

(Received 18 August 2015; revised manuscript received 4 May 2016; published 14 July 2016)

To demonstrate that phase separation is a main mechanism of pattern formation for one of the spatiotemporal patterns emerging in the Ag and Sb electrodeposition system, I performed numerical simulations to model the mixed system of conductive and insulative materials under a steady electric field. For such a dissipative system, I derived the extended Cahn-Hilliard equation using Onsager's variational principle. My results demonstrate that conductive and insulative materials phase separate spatially under the constant-current mode.

DOI: [10.1103/PhysRevE.94.010203](https://doi.org/10.1103/PhysRevE.94.010203)

It is expected that spatiotemporal patterns are formed, which are accompanied by phase separations, under thermodynamically open conditions where energy and/or materials are continuously supplied to, and dissipated out from, the system [1,2]. Such a spatiotemporal phenomenon can be considered as a new class of physical systems, similar to the currently adopted theoretical frameworks such as reaction-diffusion systems [3] or relaxation kinetics of phase segregation [4]. In general, biological life is maintained as neither a simple reaction-diffusion system nor a monotonous relaxation system. In this sense, spatiotemporal patterns can exhibit some similarities with the unrevealed biological phenomenon in its essential aspect.

The Ag and Sb co-electrodeposition system, in which Ag and Sb atoms consistently accumulate on an electrode surface from a solution during electrodeposition [5–10], exhibits spatiotemporal behavior in a nonequilibrium system. In this system, various spatiotemporal patterns are formed on the electrode surface during electrodeposition, depending on the experimental conditions and distribution of light and dark regions. However, the mechanism that underlies the emergence of these patterns has not yet been adequately clarified. Recently, we investigated the mechanism of pattern formation for one traveling stripe pattern among the various kinds of patterns emerging in the Ag and Sb electrodeposition system. The pattern we investigated was the complex labyrinthine structure, which intriguingly is formed by metals. According to our static element analysis, the light and dark stripes of the pattern are rich in Ag and Sb, respectively [7]. In our previous report concerning the time evolution of stripe width, the phase separation of Ag and Sb in the electrodeposition system was suggested as a plausible pattern formation mechanism of the complex labyrinthine structure [8]. Our *in situ* real-time element imaging uses radiation to show that Ag separates spatially with the stripe shape and the Ag-rich stripes propagate [10], and the result suggests validity for the mechanism mentioned above.

Ag and Sb possess conductive and (relatively) insulative properties, respectively. The resistivities of Ag ( $1.63 \mu\Omega \text{ cm}$ ) and Sb ( $40.1 \mu\Omega \text{ cm}$ ) at  $20^\circ \text{C}$  differ by a factor of 25 [11]. If the phase separation between these materials actually contributes to the mechanism of pattern formation, the phase separation

might be induced by the difference between their resistivities, as well as the conventional phase separation induced by the forces of attraction between the same materials and of repulsion between different materials. Consequently, in the resultant pattern, Ag and Sb with very different resistivities are respectively concentrated in the light and dark stripes [7]. Therefore, in this study, I used numerical simulations to determine whether the conductive and insulative properties of Ag and Sb, when subjected to an electric field, induce a phase separation.

The system considered here is shown in Fig. 1. Two electrodes are immersed in the electrolyte solution, and Ag and Sb adsorb on one electrode surface to form a film. The electromotive force is  $E$  and the flowing current in the electric circuit is  $I$ . In this study, the constant-current mode (the galvanostat mode) is considered, where  $I_0$  is a constant. This mode is considered because the complex labyrinthine structure of the used materials, whose pattern mechanism is speculated to be the phase separation, is formed under the constant-current mode in the experimental system of Ag and Sb electrodeposition. Under the constant-current mode, the value of  $E$  is automatically adjusted following an environmental change in order to maintain a constant current value  $I_0$ . The entire resistance of the film on the electrode surface is  $R$ . The area from the surface of the film to the counter electrode corresponds to the electrolyte solution. The resistivity of the film-forming materials A and B are  $R_A$  and  $R_B$ , respectively. Here, the relation of  $R_A = gR_B$  holds, where  $g$  is positive and more than 1. Thus, material A is insulative and material B is conductive. For simplicity, one-dimensional electrodes are assumed and, along the electrode, the  $x$  coordinate is used. The concentrations of the respective materials A and B at position  $x$  and time  $t$  are  $C_A(x, t)$  and  $C_B(x, t)$ .

Using Onsager's variational principle [12], the function  $Q$  to be minimized in the dissipative system is the sum of the free energy of the system and the consumption energy emerging when the current flows to the film:

$$Q(C_A(x, t)) = \int \left[ \frac{\varepsilon^2}{2} (\nabla C_A)^2 + W(C_A) \right] dx + \frac{1}{2} R I_0^2. \quad (1)$$

The first term of the right side is the interfacial energy to reduce the concentration variation and avoid the interface formation, while  $\varepsilon$  is a coefficient.  $W(C_A)$  represents the internal energy and the entropy of the system. The sum of the first and second terms is the free energy for the system. The third term shows the consumption energy emerging from the resistance of the

\*ynagamin@ube-k.ac.jp

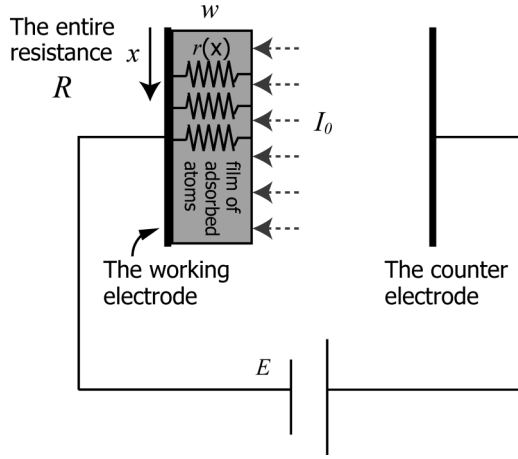


FIG. 1. Schematic drawing of the film formed by the insulative and conductive materials A and B under the constant-current mode.

electrodeposited film under the current. It is a dissipative energy term [12]. The entire resistance  $R$  is written such that  $R = 1/\int \frac{1}{r(x)} dx$ , which assumes that local resistances  $r(x)$  are parallelly put onto the  $x$  axis (Fig. 1). Here,

$$r(x) = A_0[R_A C_A(x) + R_B C_B(x)]w, \quad (2)$$

where  $A_0$  is a coefficient and  $w$  is a thickness of the film. To examine the time evolution of the concentration, the extended Cahn-Hilliard equation of this system was described using the function  $Q$ , as below. Since the concentration is a conserved quantity, the equation of the continuity holds:

$$\frac{\partial C_A(x,t)}{\partial t} = -\text{div } \vec{J}, \quad (3)$$

where  $\vec{J}$  is the mass flux. Moreover,  $Q$  can be transformed to

$$Q(C_A(x,t)) = \int \left[ \frac{\varepsilon^2}{2} (\nabla C_A)^2 + W(C_A) + \bar{f} \right] dx. \quad (4)$$

$\bar{f}(\{r(x),t\})$  is a function that spatially averages the consumption energy of the third term and is defined as

$$\int \bar{f}(\{r(x),t\}) dx = \frac{1}{2} R I_0^2 = \frac{1}{2} \left[ 1 / \int \frac{1}{r(x)} dx \right] I_0^2. \quad (5)$$

Here, two conserved conditions of the concentration are imposed:

$$\int C_A(x,t) dx = \text{const} \quad \text{at all time}, \quad (6)$$

$$C_A(x,t) + C_B(x,t) = \text{const} \quad \text{at all time}. \quad (7)$$

For convenience, in this study  $C_A(x,t) + C_B(x,t)$  is assumed to be 1 in Eq. (7).

If it is assumed that  $\vec{J} = -L\nabla\left(\frac{\delta q}{\delta C_A}\right)$  [13], where  $q$  is an integrand of the right side of Eq. (4) [ $q = \frac{\varepsilon^2}{2} (\nabla C_A)^2 + W(C_A) + \bar{f}$ ] and  $L$  is a positive constant, the continuity equation (3) becomes

$$\frac{\partial C_A(x,t)}{\partial t} = L\nabla^2 \left( \frac{\delta q}{\delta C_A} \right). \quad (8)$$

Inserting  $q$  into Eq. (8) gives

$$\begin{aligned} \frac{\partial C_A(x,t)}{\partial t} = L\nabla^2 \left( -\varepsilon^2 \nabla^2 C_A(x) + \frac{dW}{dC_A(x)} \right) \\ + L\nabla^2 \frac{d\bar{f}(\{C_A(x),t\})}{dC_A(x)}. \end{aligned} \quad (9)$$

The Ginzburg-Landau style is used to express  $W(C_A)$ , where  $W(C_A) = -a[C_A(x) - 0.5]^2 + b[C_A(x) - 0.5]^4$ , where  $a$  and  $b$  are positive coefficients.  $W(C_A)$  includes the internal energy by considering the affinity between the molecules of the same material and the repellent effect between molecules of different materials, which drives a conventional phase separation. Thus, Eq. (9) without the third term of the right side is the conventional Cahn-Hilliard equation describing phase separation, also called spinodal decomposition [13,14]. From Eqs. (2) and (5),  $\bar{f}$  used in the third term of the right side of Eq. (9) is in detail written as follows:  $\bar{f}(\{C_A(x),t\}) = \frac{1}{2l} \left[ 1 / \int \frac{1}{A_0[R_A C_A(x) + R_B C_B(x)]w} dx \right] I_0^2$ , where  $l$  is the total length of  $x$ . In my calculation, 80 cells denoting the concentration at the local position of the electrode with total length  $l$ , two are set on the one-dimensional ( $x$ ) axis. Based on the requirement for spatial global coupling of the concentrations [as derived from the conserved rule of Eq. (6) and for the total concentration over the entire space to be kept constant], when the time evolution of concentration  $C_A^i$  of the  $i$ th cell is calculated, the  $j$ th cell is randomly chosen by generating the random number to calculate the term  $\frac{\Delta \bar{f}}{\Delta C_A^i} \approx \frac{d\bar{f}}{dC_A(x)}$  in the third term of the right side for Eq. (9). It is set that while  $C_A^i$  is altered by a small variation  $\Delta C_A^i$ ,  $C_A^j$  is varied by  $\Delta C_A^j (= -\Delta C_A^i)$  via the conservation rule [Eq. (6)]. The local resistances  $r^i$  and  $r^j$  are respectively recalculated depending on the concentration changes of  $C_A^i$  and  $C_A^j$  [Eq. (2)], and  $\Delta \bar{f} = \bar{f}|_{C_A^i=C_A^i+\Delta C_A^i} - \bar{f}|_{C_A^i=C_A^i}$  is calculated. At each step of calculating Eq. (9), a concentration fluctuation of size  $\leq 10^{-3}$  is added using a random number. In the calculation for the cells at the boundary, the periodic boundary condition is introduced.

Next, if  $Q$  is expressed as

$$\frac{dQ}{dt} = \int \frac{\delta q}{\delta C_A} \frac{\partial C_A}{\partial t} dx \quad (10)$$

and the continuity in Eq. (3) is substituted into Eq. (10), I obtain

$$\frac{dQ}{dt} = \int \frac{\delta q}{\delta C_A} (-\text{div } \vec{J}) dx \quad (11)$$

Furthermore, if the right side of Eq. (11) is integrated by parts, assuming zero flux at the boundary limit, it becomes

$$\frac{dQ}{dt} = \int \nabla \cdot \left( \frac{\delta q}{\delta C_A} \vec{J} \right) dx. \quad (12)$$

If the precondition formula  $\vec{J} = -L\nabla\left(\frac{\delta q}{\delta C_A}\right)$  used in Eq. (9) is substituted into Eq. (12), the condition of  $dQ/dt \leq 0$  holds. Namely, if Eq. (9), which is introduced with a prior condition of  $\vec{J} = -L\nabla\left(\frac{\delta q}{\delta C_A}\right)$ , is calculated,  $Q$  is inevitably minimized with time, and Onsager's variational principle that the sum of the free energy and the dissipative energy should be minimized with time [13] is fulfilled.

Comparing the above extended Cahn-Hilliard equation [Eq. (9)] and the conventional Cahn-Hilliard equation without

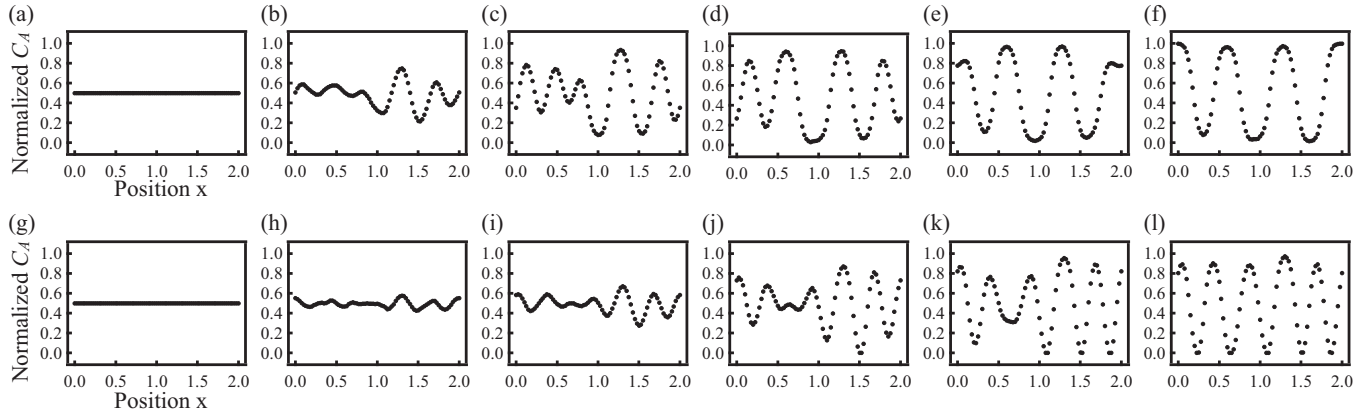


FIG. 2. Time evolution of the calculation derived from the numerical simulation using Eq. (9). Step time is  $\Delta t = 3.0 \times 10^{-7}$ . Maximum steps are  $6.0 \times 10^5$ .  $a = 0.5$ .  $b = 1.0$ .  $\varepsilon = 0.05$ . The initial concentration of  $C_A$ ,  $C_{\text{int}} = 0.5$ .  $L = 1.0$ . (a)–(f) The conventional Cahn-Hilliard equation without the consumption energy [the last term in Eq. (9)] emerging by the resistance of the film. (a) 0th step. (b)  $1.0 \times 10^5$ th step. (c)  $2.0 \times 10^5$ th step. (d)  $3.0 \times 10^5$ th step. (e)  $5.0 \times 10^5$ th step. (f)  $6.0 \times 10^5$ th step. At  $5.6 \times 10^5$ th step, the phase separation is completed and, until the  $6.0 \times 10^5$ th step, the condition is stable. (g)–(l) The extended Cahn-Hilliard equation (9) including the consumption energy emerging by the resistance of the film under the constant-current mode.  $I_0 = 2.1$ .  $A_0 w R_A = 5.0$ .  $A_0 w R_B = 1.0$ . Therefore, the ratio of resistivity of  $R_A$  to  $R_B$  is 5.0. (g) 0th step. (h)  $2.50 \times 10^4$ th step. (i)  $5.00 \times 10^4$ th step. (j)  $7.50 \times 10^4$ th step. (k)  $1.00 \times 10^5$ th step. (l)  $1.25 \times 10^5$ th step.

the third term, at the time when the phase separation does not yet occur in the conventional Cahn-Hilliard equation [Fig. 2(a)], the phase separation already begins in the extended Cahn-Hilliard equation with the third term of the consumption energy [at the  $2.5 \times 10^4$ th step, Fig. 2(h)]. This indicates that the consumption energy of the third term induces the phase separation of the materials by utilizing the difference between resistivities of the materials. The characteristic peculiar to the extended Cahn-Hilliard equation is a tendency to reach 0.0 in a local minimum of  $C_A$  [Fig. 2(l)], comparing it to the conventional Cahn-Hilliard equation [Fig. 2(f)]. In the conventional Cahn-Hilliard equation, the local minima values of  $C_A$  (the positions of  $x$  are around 0.3, 0.9, and 1.6) are  $\sim 0.1$  after the phase separation is completed at the  $6.0 \times 10^5$ th step [Fig. 2(f)]. However, the extended Cahn-Hilliard equation [after the  $1.25 \times 10^5$ th step of Fig. 2(l)] has five infinitesimals (the positions  $x$  are around 0.25, 0.6, 1.1, 1.5, and 1.9) and the positions of the infinitesimals are +2 greater than those in the conventional Cahn-Hilliard equation. In addition, the values at the infinitesimals reach zero.

Figure 3 shows the time evolution of the total resistance  $R$  calculated in the numerical simulation shown in Figs. 2(g)–2(l). As time passes, material A is spatially separated from the uniform distribution, and at some positions the concentration  $C_A$  becomes 0.0. The positions  $x$  are around 0.25, 0.6, 1.1, 1.5, and 1.9. The arrows of Fig. 3 indicate that the concentration distribution has one or two additional local minima of  $C_A$ . Every time  $C_A$  reaches 0.0 at the local position, the value of  $R$  suddenly becomes lower. Consequently, the consumption energy  $\frac{1}{2} R I_0^2$  of the last term in Eq. (1) substantially decreases. It turns out that the dissipative energy is minimized.

If the ratio of resistivities for  $R_A$  to  $R_B$  is set to be larger than that in Fig. 3, when the local minimum value of  $C_A$  reaches zero, the calculated results indicate they possess an explosive behavior and become unstable. Due to the high resistivity ratio, this further enhances a dramatic decrease in the value of  $\frac{1}{2} R I_0^2$  when  $C_A$  reaches zero, as mentioned above.

On the other hand, under the constant-voltage mode (the constant-potentiostat mode), the function  $Q$  to be minimized in the dissipative system is

$$Q(C_A(x,t)) = \int \left[ \frac{\varepsilon^2}{2} (\nabla C_A)^2 + W(C_A) \right] dx + \frac{1}{2} \frac{E_0^2}{R}, \quad (13)$$

where  $E_0$  is the constant voltage applied to the electrode. Under the constant-voltage mode, the flowing current  $I$  is altered with circumstantial changes, to maintain a constant voltage  $E_0$ . If it is assumed that  $Q = \int \left[ \frac{\varepsilon^2}{2} (\nabla C_A)^2 + W(C_A) + \bar{f}_E \right] dx$ , then

$$\begin{aligned} \frac{1}{2} \frac{E_0^2}{R} &= \frac{1}{2} \int \frac{1}{r(x)} dx E_0^2 = \int \frac{E_0^2}{2r(x)} dx = \int \bar{f}_E dx, \\ \bar{f}_E &= \frac{E_0^2}{2r(x)}, \end{aligned} \quad (14)$$

where  $\bar{f}_E$  is expressed in terms of a local resistance  $r(x)$ . Based on the above relation, the extended Cahn-Hilliard equation

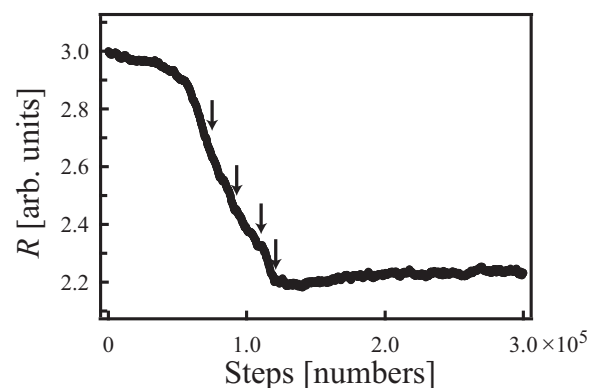


FIG. 3. Time evolution of the entire resistance  $R$  of the film under the constant-current mode, using the extended Cahn-Hilliard equation [Eq. (9)]. The parameters are the same as those of Figs. 2(g)–2(l).

under the constant voltage mode is written as

$$\frac{\partial C_A(x)}{\partial t} = L\nabla^2\left(-\varepsilon^2\nabla^2 C_A + \frac{dW}{dC_A}\right) + \frac{LE_0^2}{2}\nabla^2\frac{d(1/r(x))}{dC_A}. \quad (15)$$

Equation (15) indicates that under the constant-voltage mode, there is no spatial global coupling. This is quite different from the constant-current mode. If the detailed expression of  $r(x)$  is substituted into Eq. (15), I obtain

$$\frac{\partial C_A(x)}{\partial t} = L\nabla^2\left(-\varepsilon^2\nabla^2 C_A + \frac{dW}{dC_A}\right) + \frac{LE_0^2}{2A_0W}\nabla^2\frac{-(R_A - R_B)}{[(R_A - R_B)C_A + R_B]^2}, \quad (16)$$

where  $-(R_A - R_B)$  is negative because  $R_A = gR_B$ . The term for  $\frac{1}{[(R_A - R_B)C_A + R_B]^2}$  is positive and is a monotonically decreasing function against  $C_A$ . If  $C_A(x)$  locally protrudes or dents on the  $x$  axis, the values of  $\nabla^2\frac{1}{[(R_A - R_B)C_A + R_B]^2}$  are convex with a positive sign on the maximum position or concave with a negative sign on the minimum position, against  $x$ , in conjunction with the  $C_A(x)$  distribution. However, since the sign for  $-(R_A - R_B)\frac{LE_0^2}{2A_0W}$  is negative, then  $-(R_A - R_B)\frac{LE_0^2}{2A_0W}\nabla^2\frac{1}{[(R_A - R_B)C_A + R_B]^2}$  [i.e., the last term of Eq. (16)] becomes concave (with a negative sign on the minimum position) or convex (with a positive sign on the maximum position) inversely with the  $C_A(x)$  distribution. Namely, if  $C_A(x)$  fluctuates spatially, deviating from the uniform distribution, the third term (the dissipative term) acts on the system to keep a uniform distribution of  $C_A(x)$ . Under the constant-voltage mode, the difference of the resistivities between the conductive and the insulative materials has the tendency to suppress phase separation. Actually, in the numerical simulation using Eq. (15), a phase separation was not observed even when the parameters were varied.

To conclude, this study suggests a new formulation, an extended Cahn-Hilliard equation, using Onsager's variational principal, to investigate the dynamics of the concentration distribution under a dissipative system. My calculations

demonstrate that a phase separation of the conductive and insulative materials is induced under the constant-current mode, but is suppressed under the constant-voltage mode. According to our experimental observations of the Ag and Sb electrodeposition system, the complex labyrinthine structure, which I model using a numerical simulation, emerges in the wide range of the current values under the constant-current mode. Under the constant-voltage mode, the complex labyrinthine structure rarely appears [6,15]. This experimental tendency supports the results of my numerical calculations using the extended Cahn-Hilliard equation. Conversely, the results have differences from the experimental result. While the width of the phase-separated stripe becomes constant with time in the numerical result under the constant-current mode, the stripe width became bigger with time in the experimental system [8]. It might be caused by the condition for numerical simulation that this model does not account for the continuous adsorption of metal atoms from the electrolyte solution to the electrode surface processed in the real experimental system of the Ag and Sb electrodeposition.

Furthermore, in this study, two-dimensional numerical simulation considering a real electrode surface shape is not carried out [16,17]. However, the previous theoretical model postulates the diffusion-reaction system which is driven by the oxidation reduction of one element, for example, Fe, as a mechanism of a pattern formation. The reaction-diffusion system could not explain the phase separation of two elements, for example, Ag and Sb, which is one of experimental results of the complex labyrinthine structure [7]. The result obtained by this model is the first step to proving that phase separation is a main mechanism of the complex labyrinthine structure. Moreover, when considering other systems, my model has the potential to be applied to other phenomena, such as cases where ion doping enhances the block copolymer alignment under an electric field [18]. Furthermore, this model could also explain the spatiotemporal pattern formation in biological systems, such as the division of a cell nucleus.

My work was supported, in part, by Grants-in-Aids for Challenging Exploratory Research, JSPS KAKENHI (No. 25610106).

- 
- [1] T. Okuzono and T. Ohta, *Phys. Rev. E* **67**, 056211 (2003).  
 [2] M. Hildebrand, A. S. Mikhailov, and G. Ertl, *Phys. Rev. Lett.* **81**, 2602 (1998).  
 [3] A. N. Zaikin and A. M. Zhabotinsky, *Nature* **225**, 535 (1970).  
 [4] Y. Oono and S. Puri, *Phys. Rev. A* **38**, 434 (1988).  
 [5] I. Krastev and M. T. M. Koper, *Physica A* **213**, 199 (1995).  
 [6] Y. Nagamine and M. Hara, *Physica A* **327**, 249 (2003).  
 [7] Y. Nagamine and M. Hara, *Phys. Rev. E* **72**, 016201 (2005).  
 [8] Y. Nagamine and M. Hara, *Surf. Sci.* **601**, 803 (2007).  
 [9] Y. Nagamine and K. Yoshikawa, *Chaos* **20**, 023117 (2010).  
 [10] Y. Nagamine and K. Yoshikawa (unpublished).  
 [11] *Metals Reference Book*, edited by C. J. Smithells (Butterworths, London, 1976), pp. 940–941.  
 [12] L. Onsager, *Phys. Rev.* **37**, 405 (1931).  
 [13] J. W. Cahn, *Acta Metall.* **9**, 795 (1961).  
 [14] J. W. Cahn and J. E. Hilliard, *J. Chem. Phys.* **28**, 258 (1958).  
 [15] Y. Nagamine (unpublished).  
 [16] B. Bozzini, D. Lacitignola, and I. Sgura, *J. Solid State Electrochem.* **17**, 467 (2013).  
 [17] B. Bozzini, G. Gambino, D. Lacitignola, S. Lupo, and M. Sammartino, *Comput. Math. Appl.* **70**, 1948 (2015).  
 [18] J.-Y. Wang, T. Xu, J. M. Leiston-Belanger, S. Gupta, and T. P. Russell, *Phys. Rev. Lett.* **96**, 128301 (2006).